JOURNAL OF CATALYSIS **161,** 798–809 (1996)
ARTICLE NO. 0243

Kinetic Modeling of *n*-Hexane Oxyfunctionalization by Hydrogen Peroxide on Titanium Silicalites of MEL Structure (TS-2)

J. E. Gallot, H. Fu, M. P. Kapoor, and S. Kaliaguine[1]

Département de Génie Chimique, Université Laval, Ste-Foy, Québec, G1K 7P4, Canada

Received December 29, 1995; revised February 26, 1996; accepted March 18, 1996

Catalytic oxyfunctionalization of *n*-hexane by aqueous H_2O_2 is a complex multiphase reaction. The kinetic modeling of a set of catalytic reaction experiments performed in a batch reactor in the presence of various solvents was achieved. In the present report, a two-phase kinetic model describing the influence of these cosolvents (methanol, acetone, and water) on the initial rates as well as rates at varying catalytic reaction times, observed in the presence of titanium silicalites of MEL structure (TS-2), was proposed. The solubility of *n*-hexane in the aqueous phase was estimated using liquid–liquid equilibrium concentrations calculated by the standard UNIQUAC model. The model is based on a simple description of the selective oxidation reaction mechanism of *n*-hexane on TS-2. The kinetic, derived assuming pseudo-steady-state conditions and no mass transfer limitations, showed second-order reaction rates with respect to H_2O_2 concentration in the aqueous phase. The complete absence of activation of the primary carbon was also discussed.

INTRODUCTION

Environmentally and economically beneficial catalytic processes of alkanes oxidation by aqueous hydrogen peroxide (30 wt%) have recently attracted the attention of many researchers. Since the byproducts of H_2O_2 decomposition are water and oxygen and since the oxidation takes place under mild conditions (<100°C), these processes have an interesting potential for industrial application.

Since the discovery of the catalytic effect of titanium silicalites in these processes (1, 2), the literature has mostly dealt with either the identification and characterization of active sites (3–15) or the experimental determination of conversion and selectivity data under specific conditions (16–20). Very few studies have, however, examined the mechanistic details (21) of these partial oxidation reactions using a kinetic analysis (22). Such analysis would nevertheless be necessary for the rational choice of industrial operating conditions and the design of an optimized large-scale catalytic reactor. The exploitation of the kinetic data is, however, not straightforward because the system is normally involving two liquid phases in addition to the solid catalyst phase. It is of course possible to increase the cosolvent concentration in order to achieve the one-liquid-phase system (23), but the reactant concentrations reached are not representative of the industrial-scale conditions. The conversion and selectivity results are indeed different depending on the number of liquid phases (24).

In a previous work (22), we have reported experimental data showing the influence of both the nature and the content of cosolvent on the time evolution of the conversions and selectivities of the oxyfunctionalization of *n*-hexane by dilute hydrogen peroxide in the presence of TS-2. A kinetic analysis of the initial rates was performed in spite of the fact that only limited *n*-hexane solubility in the aqueous phase data were available. In the present work, we have performed an extensive calculation of the equilibrium concentrations using the UNIQUAC standard model. These estimations were made under the conditions of the reported experiments (22), namely in the *n*-hexane–water biphasic system both in the absence and in the presence of methanol and acetone as cosolvents.

The objectives of the present work were therefore to combine the reported kinetic data and these thermodynamic calculations to reexamine the kinetic analysis in order to represent the time-dependent reaction rate and establish a plausible reaction mechanism for the selective oxidation of *n*-hexane over TS-2. This mechanism should account for the complete absence of activation of the primary carbon (17, 18, 21).

LITERATURE REVIEW

(a) Nature of Active Sites

Several surface characterization techniques have been used to investigate the nature of the active sites in titanium silicates catalysts. X-ray diffraction (XRD) studies indicated linear changes in unit cell parameters of the various TS catalysts (8, 10). A tetrahedral coordination of titanium in framework lattice was proposed (4), and an incorporation limit of about 2.5 Ti/uc was also observed (10). In a recent paper involving X-ray absorption near

[1] To whom correspondence should be addressed.

0021-9517/96 $18.00

edge structure (XANES) spectra of TS-1 (34), the limit of the lattice incorporation of titanium was established to be 1.7 Ti/(Ti + Si)%. Beyond this limit, a part of titanium was segregated in the amorphous phase and extraframework species could be detected. Higher incorporation limit values claimed, for example, by Thangaraj *et al.* (33) are likely due to extraframework Ti. UV–vis spectroscopy and X-ray photoelectron spectroscopy (XPS) were commonly used to probe the presence of the framework and extraframework titanium. Pure TS catalysts with a titanium content below the incorporation limit exhibit a single UV–vis band at 220 nm, corresponding to the charge transfer between Ti^{4+} ions and oxygen atoms of the lattice. This band has been ascribed to isolated framework titanium in tetrahedral coordination (4). A broad shoulder around 270 nm has been attributed to the hexacoordinated titanium species (43) and a band at 330 nm, characteristic of anatase TiO_2, could be observed at higher titanium contents. In the XPS spectra, the high binding energy doublet with Ti $2p_{3/2}$ close to 460 eV was assigned to Ti species in a tetrahedral coordination (39) and the low binding energy close to 458 eV to Ti in octahedral coordination (44).

The coordination number of titanium grafted to the silicalite lattice is still a matter of debate. In contrast with the previously proposed tetrahedral coordination of titanium, Behrens *et al.* (7) showed from XANES and from extended X-ray absorption fine structure (EXAFS) investigations of a TS catalyst with undisclosed Ti content that titanium is mainly octahedrally coordinated, even though small amounts of tetrahedral and square pyramidal Ti were detected. However, Lopez *et al.* (30) found from EXAFS analyses that the coordination number of titanium depends on the hydration state of the solid catalysts. Indeed, according to these authors, hydrated TS catalysts contain octahedrally coordinated titanium and dehydration transforms the titanium from octahedrally to tetrahedrally coordinated. Similar results were reported by Bonneviot *et al.* (31) who concluded that hydration led to an increase of the titanium coordination number from 4 to 6. Further support to tetrahedral coordination of Ti was also developed by Tuel *et al.* (6). They investigated the ESR spectra of Ti^{3+} obtained by reducing with CO the Ti^{4+} in TS-1. They attributed the observed ESR signal to the Ti^{3+} species in tetrahedral coordination, indicating that the precursor Ti^{4+} was indeed in a T site.

EXAFS spectroscopy has been also employed to characterize the local environment of the titanium ion Ti^{4+} in TS catalysts. The interpretation of Fourier-transformed peaks, based on a curve-fitting procedure, raises, however, a still open discussion: are titanium ions located at tetrahedral sites of the framework or are they defects of the crystal structure involving edge sharing of $[TiO_4]$ tetrahedra with $[SiO_4]$ tetrahedral units. The first argument was supported by Pei *et al.* (25). They found that the titanium atom in TS-1 was coordinated with four oxygen atoms at the distance of 1.80 Å. The latter was postulated by Trong On *et al.* (9, 12). A double oxo bridge between Ti and Si with Ti–Si bond distance about 2.2–2.3 Å was proposed as framework defect. In a more recent work, Le Noc *et al.* (36) have made a multiple scattering analysis of the EXAFS signal obtained at Ti K-edge X-ray absorption of low Ti content (<1.5%) TS-1. They concluded that the titanium occupies a substitutional site characterized by Ti–O–Si bond angle and Si–O distances consistent with a lattice expansion. Quantitative ^{29}Si and ^{1}H MAS NMR results indicate the presence of new TiOH groups and a redistribution of the internal SiOH groups.

As reported recently by Tuel *et al.*, the presence of sodium (Na/Ti = 2) in the gel during crystallization is affecting the titanium environment in different ways (44). Thus, catalysts prepared following the original method of Taramasso *et al.* (1) have dominantly octahedral titanium with a relatively small fraction of tetrahedral titanium. Even after HCl acid leaching, the dominant octahedral titanium still remains, suggesting the presence of non-acid-extractable extraframework Ti species, which are believed to the active in the decompositon of H_2O_2 (39). However, when the Thangaraj method (33) of preparation was used or when only minor Na amounts (Na/Ti = 0.5 in the gel) was involved in the Taramasso method, opposite effects were observed. In fact, tetrahedral titanium became dominant and less affected by the presence of Na. The authors suggested that in this case, Na^+ is adsorbed by electrostatic attraction on the negatively charged oxygen atom in the Si–O–Ti bridge. Obviously, these Na^+ ions are easily desorbed during the acid leaching. Catalyst synthesis procedures should be examined carefully when analyzing the reported characterization results of TS catalysts (38).

In order to elucidate the incorporation of titanium into framework lattice, vibrational spectroscopies including infrared (IR) and Raman were used. It has been widely reported that TS catalysts exhibit an IR band at 960–970 cm^{-1} and its intensity linearly increases with Ti content (8, 9, 11, 13). Originally, the IR intensity band at 960 cm^{-1} was ascribed to the titanyl group (3). Huybrechts *et al.* (11, 17, 27) gave support to this assignment from the reversible change in intensity of the 960 cm^{-1} band upon adsorption/desorption of H_2O_2. However, extended X-ray absorption studies conducted by Trong On *et al.* (9) showed the absence of any Ti=O bonds even though the 960 cm^{-1} IR band was still present. In contrast with the formerly proposed titanyl structure, Boccuti *et al.* (4) came to the conclusion that the 960 cm^{-1} IR peak is due to a local stretching vibration mode of the $[SiO_4]$ tetrahedral unit linked to a titanium Ti^{4+} ion. The decrease of the 960 cm^{-1} IR band intensity in the presence of Na (39, 44) at a constant titanium content gave some arguments refuting a previous interpretation involving the vibration mode of the $SiO^{\delta-}$–$Ti^{\delta+}$ (4). It has

been reported that Na^+ ions were most likely perturbing the vibration frequency of SiO^- group in the vicinity of a titanium atom (44). Indeed, Camblor *et al.* ascribed the IR absorption band at 960 cm^{-1} to a vibration mode of a SiO^- group in a Si–O–Ti bridge (37). A similar conclusion was also reached for the interpretation of the 960 cm^{-1} Raman band observed on TS-1 catalysts (14).

(b) Reaction Mechanism

The oxidation reaction mechanism of hydrocarbons by aqueous H_2O_2 on TS catalysts should clarify the path by which oxygen transfers (41) from the peroxide to the products via the catalytic site. The few publications in this field indicate the complexity of the mechanism. Up to now, the proposed reaction mechanisms can be divided in two main groups. The first one is the homolytic reaction mechanism giving rise to radical intermediates. The second group is the nonradical reaction mechanism involving an electrophilic reaction followed or not by an heterolytic cleavage of the C–H bond.

(i) Homolytic mechanism. This is the more often proposed reaction mechanism for the oxidation of alkanes, olefins, and aromatics by aqueous H_2O_2 on TS catalysts. Huybrechts *et al.* (11, 17) postulated that alkane oxyfunctionalization proceeds through a homolytic reaction mechanism and follows the reactivity: tertiary C–H > secondary C–H $\gg$ primary C–H, which is the usual stability order of the corresponding radicals. Clerici (18) supported the idea that a five-member cyclic structure with electrophilic properties was formed by a titanium hydroperoxo and a protic molecule at Ti species. This structure abstracts homolytically a hydrogen atom from the alkane C–H bond. The radical which is formed is rapidly hydroxylated to give an alcohol. Recently, Khouw and Davis (38) postulated that the alkyl radical must either have a very short life time or be sterically restricted within the zeolite.

(ii) Nonradical heterolytic/electrophylic mechanism. Huybrechts *et al.* (11) proposed an alternative nonradical mechanism for the selective oxidation of alcohols, olefins, and aromatics by aqueous H_2O_2 on TS catalysts. The oxygen transfer was described in two ways. In the case of olefins and aromatics, the oxygen transfer proceeds through a five-member cyclic structure composed of peroxo titanium and one carbon–carbon bond. Clerici and Ingallina (41) suggested that the oxygen atom is transferred directly from this cyclic structure to the epoxide.

Additional information about some mechanistic aspects of the selective oxidation of hydrocarbons on TS catalysts was also obtained by studying the influence of various kinetic factors such as temperature (19, 22, 28), solvent (reactants concentration) (6, 16, 18–20, 22), crystal size (28) and titanium content (19). The main feature reported on the oxidation reaction of alkanes and alcohols by aqueous H_2O_2 on TS catalysts was the absence of activation of the primary C–H bond. Unlike the titanium silicates, Prasad Rao *et al.* (42) reported that vanadium silicalites are also able to activate the primary C–H bond of *n*-alkanes giving primary alcohols.

PHASE EQUILIBRIUM ANALYSIS

The reaction medium for the partial oxidation of *n*-hexane by aqueous H_2O_2 on TS-2 catalysts consists of three phases: an organic liquid phase containing essentially *n*-hexane, some of the solvent, and the reaction products (2- and 3-)hexanol, (2- and 3-)hexanone; an aqueous liquid phase containing most of H_2O_2, water, and solvent; and finally, the solid catalyst. Assuming that the catalytic oxidation reaction takes place in the aqueous phase (22), only the processes at the solid–aqueous phase interface are directly involved in the reaction. The major problem consists in the estimation of both concentrations of *n*-hexane and H_2O_2 in the aqueous phase. Considering that the system reaches liquid–liquid equilibrium at any time when the reaction mixture is sufficiently stirred, these two concentrations will remain at the solubility equilibrium in the aqueous phase.

The solubility of *n*-hexane in water is very low. To improve the mutual solubility of the two liquid phases, the addition of a polar solvent such as methanol or acetone which are completely miscible with water is always required. The addition of the cosolvent into the system does not usually result in the formation of a homogeneous liquid phase under typical reaction conditions.

The liquid–liquid equilibrium can be predicted from appropriate models for the excess Gibbs free energy in the liquid state. In this work, the UNIQUAC (29) model which is described by the following equation was used:

$$\frac{g^E}{RT} = \sum_i x_i \ln(\Phi_i/x_i) + \frac{\omega}{2}\sum_i x_i q_i \ln(\theta_i/\Phi_i) - \sum_i q_i x_i \ln\Big(\sum_j \theta_j \tau_{ji}\Big), \quad [1]$$

where

$$\tau_{ij} = \exp(-A_{ij}/T)$$

$$\theta_i = x_i q_i \Big/ \sum_j x_j q_j$$

$$\Phi_i = x_i r_i \Big/ \sum_j x_j r_j.$$

The basic condition for phase equilibrium is the equality of fugacities of the components in the organic phase and aqueous phase. In terms of mole fractions x_i and activity

TABLE 1

UNIQUAC Parameters (29, 48, 49)

(a) Group Volume and Surface Parameters

Component	r_i	q_i
n-hexane	4.4998	3.856
Acetone	2.5735	2.336
Methanol	1.431	1.432
Water	0.92	1.40

(b) Binary Interaction Parameters A_{ij} [*K*]

System	A_{12}	A_{21}	A_{13}	A_{31}	A_{23}	A_{32}
I	562.5	191.2	1885	572	−623	−421.3
II	362.5	221.2	1885	572	938.4	−340.6

Note. (I), *n*-hexane (1)–methanol (2)–water (3); (II), *n*-hexane (1)–acetone (2)–water (3).

coefficients, γ_i, it follows that

$$\gamma_i^{HC} x_i^{HC} = \gamma_i^{W} x_i^{W} \qquad [2]$$

Considering the overall composition, z_i, and the phase (mole) fraction, β, of the total material that is present in the organic phase, the condition to be solved at equilibrium becomes

$$\sum_i \frac{z_i}{\beta + K_i(1-\beta)} - 1 = 0, \qquad [3]$$

where K_i is the equilibrium distribution coefficient defined as the ratio x_i^{W}/x_i^{HC}.

The UNIQUAC model was chosen because it is a versatile correlation and the necessary empirical parameters are available in the literature (29). The pure species parameters r_i and q_i as well as binary interaction parameters A_{ij} are listed in Table 1 for both the *n*-hexane–water–methanol and the *n*-hexane–water–acetone systems. A computer program RGIBBS (45) based on Eqs. [1]–[3] for predicting the liquid–liquid equilibrium behavior was used.

EXPERIMENTAL

The experimental setup and the physicochemical characterization (AA, XRD, FTIR, UV-visible spectroscopy, XANES, EXAFS) of the TS-2 catalyst were described and have been reported elsewhere (9, 22). *n*-Hexane of 99% purity (0.232 mole), aqueous 30 wt% solution of H_2O_2 (0.0882 mole), 0–31 g of cosolvent (methanol, water, acetone), and 500 mg of catalyst were stirred at 55°C in a Pyrex reactor equipped with a reflux condenser and a magnetic stirrer. The products collected from a sample of the organic phase were subjected to GC analysis using a DB wax capillary column. GC analysis showed that the main products of the reaction were (2- and 3-)hexanol and (2- and 3-)hexanone.

KINETIC MODELING

Reaction Mechanism

In the development of the reaction mechanism, some important aspects must be considered. They include:

1. the nature of the catalytic active sites and H_2O_2 decomposition sites;
2. the process by which molecular hydrogen peroxide adsorbs on the catalyst surface;
3. the mechanism of activation of some titanium sites during the catalytic reaction;
4. the initiation of the oxidation reaction: the way by which *n*-hexane and (2- and 3-)hexanol are activated in the vicinity of the catalytic site; and
5. the mechanism of H_2O_2 decomposition.

The reaction mechanism summarized in Scheme 1 and Eqs. [4]–[9] was derived based on the literature results concerning the surface characterization of Ti-silicalites and both on the preliminary kinetics experiments (22, 56) and on new analysis of the liquid–liquid phase equilibrium in the reaction medium. This mechanism involves two kinds of active sites: (i) site [T] is active in the oxidation of *n*-hexane and *n*-hexanol. H_2O_2 is also decomposed on site [T] following Eq. [4]. Site [T] is the framework Ti site which is in tetrahedral coordination in the dry sample. (ii) site [Z] is also active in H_2O_2 decomposition following Eqs. [8]–[9]. Site [Z] is believed to be an extraframework high coordination Ti site.

This mechanism is illustrated in Scheme 1.

Step (i) is the interaction of sites [T] with aqueous H_2O_2 to give a titanium hydroxyhydroperoxo group. Even though silicalites are commonly viewed as hydrophobic materials (55), Bellussi *et al.* (40) have established by means of IR and NMR spectroscopies that water is adsorbed on TS catalysts. Zecchina *et al.* (50) and Geobaldo *et al.* (43) using UV–vis spectroscopy have shown that titanium sites can also coordinate neutral ligands like H_2O giving rise to Ti^{IV} with a sixfold coordination. Boccuti *et al.* (4) concluded from the IR and UV–vis spectroscopy results that a high fraction of titanium sites are perturbed by H_2O. This means that as far as the small H_2O molecule is concerned, all the titanium sites are accessible (4). XANES results on dry and wet TS-1 samples obtained by Bonneviot *et al.* (31) and Lopez *et al.* (30) also point to an increased coordination of lattice Ti upon water adsorption.

Huybrechts *et al.* (27) reported that when TS is exposed to aqueous H_2O_2, the IR band at 960 cm^{-1} disappears and reappears when the catalyst is heated at 330 K. Experimental evidence of interaction of titanium sites with aqueous H_2O_2 was also demonstrated by the UV–vis spectra reported by Zecchina *et al.* (50) and Geobaldo *et al.* (43). In the presence of H_2O_2, a band at 26,000 cm^{-1} was formed and was ascribed to the characteristic absorption of the hydroperoxo group.

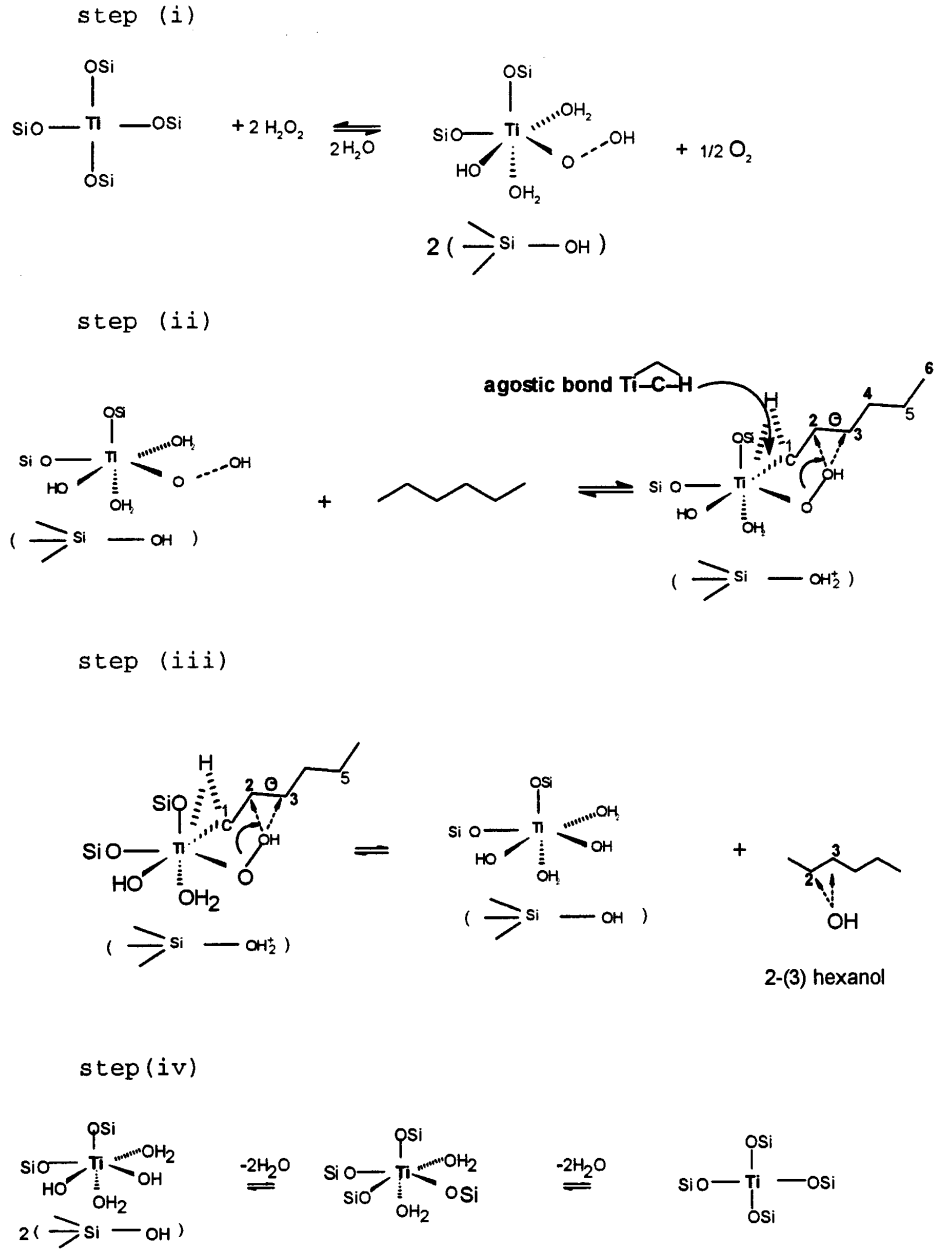

SCHEME 1

According to step (i), two molecules of H_2O_2 are required to obtain an open-type hydroxyhydroperoxo titanium [(OH)TiOOH] site with neighboring defect silanols group from the closed-type lattice Ti site (36, 51). This activation step involves the decomposition of one H_2O_2 molecule.

Step (ii) is the interaction within the zeolite pore of the aqueous *n*-hexane with the hydroxyhydroperoxo titanium. C–H bonds on hydrocarbons, particularly those of saturated (sp^3) carbon centers, are usually regarded as chemically inert. However, the work published by Brookhart and Green (52) stipulated that a carbon–hydrogen group will interact with a highly electron-deficient transition metal center like titanium with formation of a two-electron three-center bond, the so-called agostic bond. Eisenstein and Jean investigated the factors influencing such agostic bond (53). Munakata *et al.* used the density functional calculations on agostic ethyl–Ti^{IV} complexes (54). There are in fact many circumstances in organometallic compounds where the C–H group interacts with transition metal centers to form the agostic bond.

In the octahedral complex hydroxyhydroperoxo titanium site, the Ti^{4+} has an empty *d* orbital to receive the two electrons of the C–H bond of a terminal methyl. An agostic

bond of the type

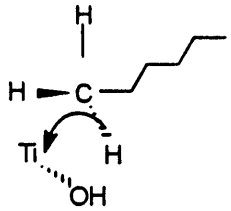

may therefore be formed at the terminal carbon of the *n*-hexane. The presence of a TiOH group in the neighborhood of the carbon and hydrogen atoms involved may be necessary to reinforce the formation of this agostic bond. Therefore, the defect silanol group in the neighborhood of the titanium site abstracts heterolytically (38) the H from the corresponding β-C or δ-C, and a complex cyclic structure of five or six members is formed in addition to the agostic Ti–C–H bond.

Step (iii) involves the corresponding formation of hexanol. The subsequent oxidation of hexanol proceeds via the same mechanism. It is interesting to note that the proposed reaction mechanism is in perfect agreement with the experimental product distributions observed during the catalytic oxidation of linear (18) and branched alkanes (38) on TS catalysts. In particular, it explains the complete absence of oxidation of the primary carbon.

Finally, in step (iv), the catalytic cycle is closed following the surface rearrangement of the hydroxy Ti sites and the silanol defects group. At the same time, during the catalytic reaction, H_2O_2 is competitively adsorbed on the extraframework $[Z]$ sites according to a dissociative chemisorption leading to H_2O_2 decomposition.

The *n*-hexane oxidation reaction mechanism on TS-2 catalyst is therefore summarized as

(a) on the framework titanium site

$$2H_2O_2 + (T) \rightleftharpoons (S1) + \tfrac{1}{2}O_2(g) \quad [4]$$

$$C_6H_{14} + (S1) \rightleftharpoons (Complex\text{-}1) \rightleftharpoons C_6H_{14}O + H_2O + (S2) \quad [5]$$

$$C_6H_{14}O + (S1) \rightleftharpoons (Complex\text{-}2) \rightleftharpoons C_6H_{12}O + H_2O + (S2) \quad [6]$$

$$(S2) \rightleftharpoons (T) + 2H_2O; \quad [7]$$

(b) on the extraframework titanium site

$$H_2O_2 + 2(Z) \rightleftharpoons 2ZOH \quad [8]$$

$$ZOH \rightarrow \tfrac{1}{2}H_2O + \tfrac{1}{4}O_2(g) + (Z). \quad [9]$$

The stoichiometric reactions corresponding to the above reaction mechanism are written as

(I) $C_6H_{14} + H_2O_2 \rightarrow C_6H_{14}O + H_2O$

(II) $C_6H_{14}O + H_2O_2 \rightarrow C_6H_{12}O + 2H_2O$

(III) $H_2O_2 \rightarrow \frac{1}{2}O_2(g) + H_2O$.

Reaction Phase Hypothesis

The treatment of kinetic data reported below was made under the assumption that the reaction takes place within the pores of the TS-2 catalyst, the solid being in contact with the aqueous H_2O_2 phase. This assumption was made following the observation that the stirred reaction medium consisted of an emulsion of bubbles of the organic phase and a distinct suspension of the catalyst particles in the aqueous phase. Moreover, when the stirring is stopped and the liquid phases are segregated, the catalyst particles remain in the aqueous phase. From our previous study of the kinetics of this reaction (56), it was also found that a change in the volume of the *n*-hexane phase did not affect the reaction rate. The significant change in the aqueous phase volume associated with the introduction of a solvent or addition of water was however yielding very important changes in the rate of reaction. Very similar observations of the effect of solvent addition on the rate of *n*-hexane conversion were also made by Tatsumi *et al.* (16) and Huybrechts *et al.* (20). These last authors concluded that this effect is explained by the opposite variations of *n*-hexane and H_2O_2 concentrations in the aqueous phase.

Rate Equations

The activation of *n*-hexane reaction on the framework titanium will be illustrated in the form of the following linear graph:

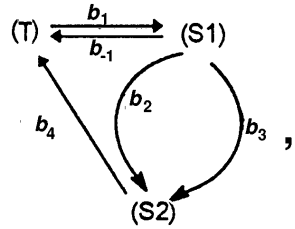

where b_1, b_2, b_3, b_4, and b_{-1} are the weights of the graph expressed as $b_1 = kc_1[H_2O_2]^2$, $b_2 = kc_2[C_6H_{14}]$, $b_3 = kc_3[C_6H_{14}O]$, $b_4 = kc_4$, and $b_{-1} = kc_{-1}$.

Assuming that the surface intermediates [T], [S1], and [S2] are in steady state, that is,

$$\frac{\partial[T]}{\partial t} = \frac{\partial[S1]}{\partial t} = \frac{\partial[S2]}{\partial t} = 0,$$

and $b_1 \ll b_2, b_3, b_4, b_{-1}$, the rates of reaction (I) and reaction (II) will be expressed as

$$r_I = \frac{k_1[H_2O_2]^2[C_6H_{14}]}{1 + K_1[C_6H_{14}] + K_2[C_6H_{14}O] + K_3[C_6H_{12}O]} \quad [10]$$

$$r_{II} = \frac{k_2[H_2O_2]^2[C_6H_{14}O]}{1 + K_1[C_6H_{14}] + K_2[C_6H_{14}O] + K_3[C_6H_{12}O]}. \quad [11]$$

At the initial time of the reaction ($t = 0$), when the concentrations of (2- and 3-)hexanol and (2- and 3-)hexanone

are still negligible, the initial rate of (2- and 3-)hexanol formation is expressed as

$$r_{I,0} = \frac{k_1[H_2O_2]^2[C_6H_{14}]}{1 + K_1[C_6H_{14}]}. \quad [12]$$

Assuming step [8] at equilibrium, the following equation will be obtained:

$$K_8 = \frac{\theta^2_{[Z(OH)]}}{\theta^2_{[Z]}[H_2O_2]}.$$

In the hypothesis that $[T]$ and $[Z]$ are different sites, the coverage of H_2O_2 decomposition sites is such as

$$\theta_{[Z]} + \theta_{[Z(OH)]} = 1.$$

Under conditions where the decomposition rate at the titanium framework sites is negligible compared to that on extraframework sites, a kinetic equation for the rate of decomposition of H_2O_2 can be obtained as

$$r_{III} = k_{c9}\theta_{[Z(OH)]}$$

$$r_{III} = \frac{k_{c9}\sqrt{K_8}[H_2O_2]^{0.5}}{1 + \sqrt{K_8}[H_2O_2]^{0.5}}.$$

At a relatively high reaction temperature, it is assumed that $(K_8[H_2O_2])^{0.5} \ll 1$; then r_{III} is simplified to

$$r_{III} = k_3[H_2O_2]^{0.5} \quad [13]$$

with $k_3 = k_{c9}(K_8)^{0.5}$.

Equations [10], [11], and [13] can describe the kinetic rates of the three independent reactions (I), (II), and (III) during the catalytic oxidation of *n*-hexane by aqueous H_2O_2.

Numerical Integration of Rate Equations

The overall reaction between the two immiscible reactants H_2O_2 and *n*-hexane on TS-2 catalyst requires different mass transfer processes. Such processes involve: (i) mass transfer of H_2O_2 from the aqueous phase to the external surface of TS-2, (ii) diffusion of H_2O_2 reactant to the interior of the catalyst pellet through pores, (iii) mass transfer of *n*-hexane from the organic phase to the interface between both liquid phases, (iv) thermodynamic phase equilibrium at the interface, (v) mass transfer of *n*-hexane reactant from the interface to the aqueous phase, (vi) mixing and diffusion of *n*-hexane in the aqueous bulk phase, (vii) mass transfer of *n*-hexane from aqueous phase to the external surface of catalyst and diffusion inside the pore volume of TS-2, (viii) intrinsic reaction of reactants with the active sites of catalyst pellets which are dispersed in the aqueous phase, (ix) diffusion of products outward to the exterior of catalyst pellet through pores, and finally, (x) mass transfer of products to the bulk solution and back to the organic phase.

In the case of negligible internal mass transfer diffusion of the reactants, the mass balance equations corresponding to the aqueous phase and the organic phase in a batch reactor system are

$$V_o\frac{dC_{i,org}}{dt} = -K_w a V_a\left[C^{(int)}_{i,a} - C_{i,a}\right] \quad [14]$$

$$V_a\frac{dC_{i,a}}{dt} = K_w a V_a\left[C^{(int)}_{i,a} - C_{i,a}\right] + (r_i)W_{cat}, \quad [15]$$

where $K_w a$ is the volumetric aqueous phase mass transfer coefficient. In the case of hydrogen peroxide mass balance where $C_{i,org} = 0$ and thus $dC_{i,org}/dt = 0$, it follows that

$$V_a\frac{dC_{i,a}}{dt} = r_i W_{cat}.$$

Writing the aqueous phase concentration of H_2O_2 as $[H_2O_2]$, the above equation becomes

$$\frac{d[H_2O_2]}{dt} = r_{H_2O_2} \cdot \frac{W_{cat}}{V_a} = R_{H_2O_2} \quad (\text{kmol/m}^3\text{h}). \quad [16]$$

Equation (16) combined with the kinetic rate expressions is rewritten using the partial conversions of H_2O_2 in the three independent reactions (I), (II), and (III) and is expressed in the following equations under the pseudo-steady-state hypothesis

$$\frac{dx_1}{dt} = \frac{k_1[C_6H_{14}][H_2O_2]^2}{[H_2O_2]_{,0}(1 + K_1[C_6H_{14}] + K_2[C_6H_{14}O]^n_{org} + K_3[C_6H_{12}O]_{org})} \quad [17]$$

$$\frac{dx_2}{dt} = \frac{k_2[C_6H_{14}O]^n_{org}[H_2O_2]^2}{[H_2O_2]_{,0}(1 + K_1[C_6H_{14}] + K_2[C_6H_{14}O]^n_{org} + K_3[C_6H_{12}O]_{org})} \quad [18]$$

$$\frac{dx_3}{dt} = 2 \cdot [H_2O_2]_0^{(m-1)} \cdot k_3(1 - x_1 - x_2 - x_3)^m, \quad [19]$$

where x_1, x_2, and x_3 are the H_2O_2 partial conversions in reactions (I), (II), and (III), respectively, and under the initial condition $t = 0$, $(x_1, x_2, x_3)^T = (0, 0, 0)^T$; $[H_2O_2]$ and $[C_6H_{14}]$ are aqueous phase concentrations; and $[C_6H_{14}O]_{org}$ and $[C_6H_{12}O]_{org}$ are organic phase concentrations expressed as $[C_6H_{12}O] = \lambda_1\,[C_6H_{12}O]_{org}$ and $[C_6H_{14}O]_{aq} = \lambda_2[C_6H_{14}O]^n_{org}$.

The three ordinary differential equations are solved numerically with the initial condition reaction by the Gear's backward differentiate formula integration method (46). The associated kinetic constants were estimated by a nonlinear regression method in the case of the initial rates data and by the modified direct search polytope algorithm (46) for the time-dependent kinetic rates data. In this case, the following objective function was minimized:

$$F_{obj} = \sum_{i=1}^{3}\sum_{j=1}^{N}\left[\left(x^{exp}_{ij} - x^{pred}_{ij}\right)/x^{exp}_{ij}\right]^2.$$

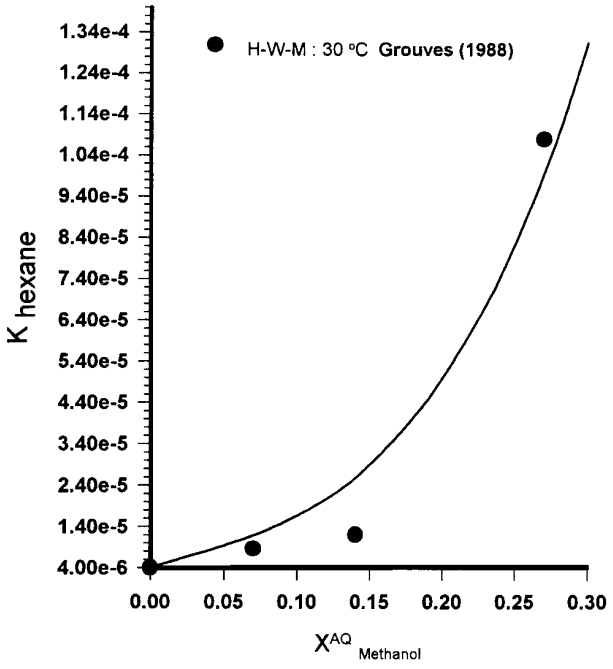

FIG. 1. *n*-hexane equilibrium partition coefficient with methanol as cosolvent. Temperature = 30°C. Solid line, predicted values; (●) Ref. (48).

RESULTS AND DISCUSSION

Simulation results for the prediction of the liquid–liquid equilibrium concentrations in the *n*-hexane–methanol–water system at 30°C are shown in Fig. 1. These results are presented in the form of the *n*-hexane equilibrium partition coefficient. The experimental data of Groves *et al.* (48) obtained under the same conditions were taken to test the validity of the predicted values. As a result, a satisfactory agreement was obtained between the computed values and the experimental points. The same UNIQUAC parameters values were used to predict the liquid–liquid equilibrium behavior of the system at the temperature of kinetic experiments, 55°C. Table 2 shows an example of the mass balance results and Fig. 2 shows the predicted concentrations of *n*-hexane and H_2O_2 in the aqueous phase as functions of the mass of cosolvents methanol and acetone added in the reactor. The addition of a solvent (methanol or acetone) to the reaction mixture results in an increase of the *n*-hexane solubility in the aqueous phase from the low solubility value in water of about 3.3×10^{-4} mol/liter to a relatively higher value in the range of 0.06–0.10 mol/liter. However, at the same time, the concentration of H_2O_2 in the aqueous phase is drastically reduced from 8.0–9.0 to 1.7–1.9 mol/liter.

Various methanol, acetone, and water contents in the 0 to 31 g range were used for the *n*-hexane oxyfunctionalization tests at 55°C, involving consequently different *n*-hexane and H_2O_2 concentrations in the aqueous phase.

The results of kinetic data measurements were first expressed as the initial rate of *n*-hexane consumption or (2- and 3-)hexanol formation. Since the kinetic model developed as Eq. [12] showed qualitative trends similar to the experimentally observed ones, its quantitative adequacy was then tested by fitting this model to the experimental initial rate data obtained with methanol as cosolvent. The kinetic parameters were estimated using the nonlinear regression method and the results are listed in Table 3 (method 1). Table 3 shows the statistical *F* and *t* values, indicating the adequacy of the model and the significance of the parameters. Figure 3 shows experimental and calculated initial rates versus H_2O_2 aqueous phase concentration, with methanol, acetone, and water as solvents at different contents. It is especially important to note that all three curves could be reasonably fitted using the same k_1 and k_2 values which appear here as independent of the cosolvent.

Figure 3 reveals that with methanol and acetone as cosolvents, initial rates of *n*-hexane consumption or (2- and 3-)hexanol formation reach a maximum at a H_2O_2 aqueous phase concentration of about 7 mol/liter. However, using water as solvent, the initial rates vary monotonously with $[H_2O_2]$ according to a second-order reaction. These observations were similar to the published work of Huybrechts and Jacobs (20) and Fu and Kaliaguine (22). The opposite variation of H_2O_2 and *n*-hexane aqueous concentrations with the addition of different amounts of solvent explain the observed maxima in the initial rate. In the *n*-hexane–water system, the solubility of *n*-hexane is independent of the amount of water; it depends only on temperature. So, according to the rate expression in Eq. [12], the initial rate of *n*-hexane conversion in the system *n*-hexane–water should only exhibit a monotonous variation

TABLE 2

Mass Balance of the Organic and Aqueous Phases under the Initial Conditions of the Kinetic Experiments (Mass of Solvent 31 g, $T = 55°C$)

(a) Hexane–Acetone–Water System

Component	Feed (kmol)	Organic phase (mole fraction)	Aqueous phase (mole fraction)
n-hexane	2.32×10^{-4}	0.942	0.349×10^{-2}
Acetone	5.34×10^{-4}	0.561×10^{-1}	0.571
Water	3.89×10^{-4}	0.670×10^{-4}	0.426
	Phase fraction:	0.210	0.790

(b) Hexane–Methanol–Water System

Component	Feed (kmol)	Organic phase (mole fraction)	Aqueous phase (mole fraction)
n-hexane	2.32×10^{-4}	0.977	2.99×10^{-3}
Methanol	9.67×10^{-4}	2.29×10^{-2}	0.710
Water	3.89×10^{-4}	8.28×10^{-5}	0.287
	Phase fraction:	0.147	0.853

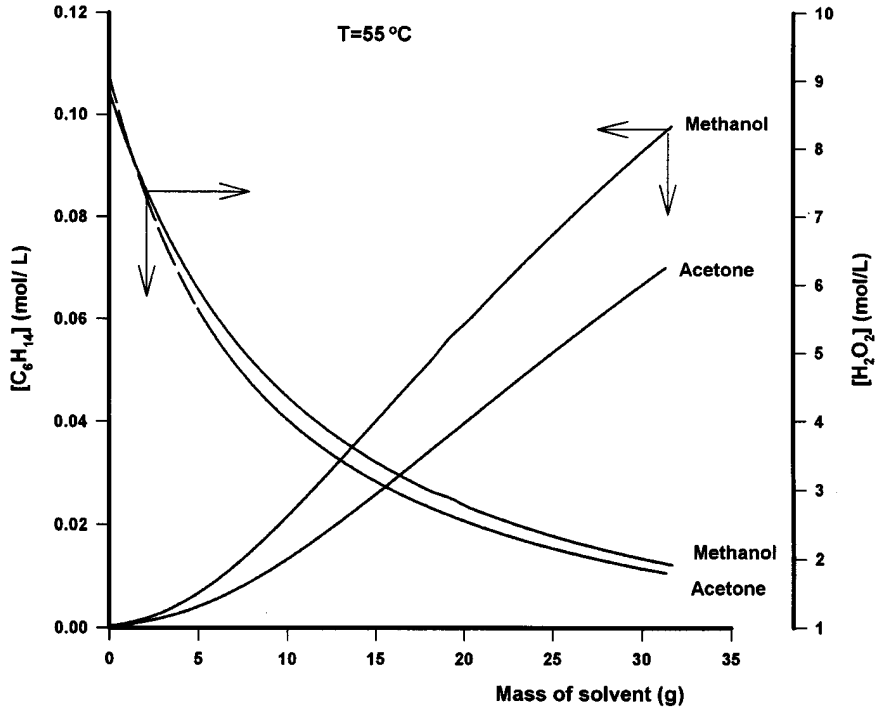

FIG. 2. Evolution of *n*-hexane and H_2O_2 concentrations in aqueous phase versus solvent amount. Temperature = 55°C.

with H_2O_2 concentration. This fact is in good agreement with the experimental data as shown in Fig. 3.

The initial ternary liquid–liquid equilibrium system becomes a complex multicomponent one involving *n*-hexane–cosolvent–water–(2- and 3-)hexanol and (2- and 3-)hexanone phase equilibrium system as the hexanol and the hexanone reaction products are gradually formed during the catalytic oxidation of *n*-hexane. Some simplifications is necessary to express the time-dependent kinetic behavior. Thus, at each reaction time step, the two liquid phases reach thermodynamic equilibrium and the equilibrium distribution coefficient of the reaction products will be assumed negligibly small. In fact, as previously observed (22), the hexanol and the hexanone prefer to stay in the organic phase environment.

The results for experimental and predicted values of partial conversions of H_2O_2 in the three parallel reactions (I)–(III) versus time of reaction are illustrated in Fig. 4,

TABLE 3

Estimated Kinetic Parameters, $T = 55°C$

				Approx. 95% confidence limits		
Method	Equations	Kinetic parameters	Estimated value	Lower	Upper	*t* value
(1)	[12]	k_1($m^6\ h^{-1}\ kmol^{-2}$)	0.954e-4	9.170e-4	1.034e-3	38.52
		K_1($m^3\ kmol^{-1}$)	1.189e3	1.095e3	1.283e3	29.18
Method	Equations	Kinetic parameters	Estimated value	Relative objective function value		
(2)	[17]–[19]	k_2($m^6\ h^{-1}\ kmol^{-2}$)	3.501×10^{-6}	8.78×10^{-2}		
		$k_3{}^a$($m^{1.5}\ kmol^{0.5}\ h^{-1}$)	4.598×10^{-2}			
		K_3($m^3\ kmol^{-1}$)	0.306			
		K_2($m^3\ kmol^{-1}$)	4.138×10^{-2}			
		m^a	0.474			
		n	0.111			

Note. (1), Parameter estimation by the nonlinear regression of Eq. [12], F value = 1333.8. (2), Parameter estimation by the modified direct search polytope algorithm.

[a] The exponent of $[H_2O_2]$ in Eq. [13] was kept as an adjustable parameter, m, and found to be equal to 0.5 within the experimental error.

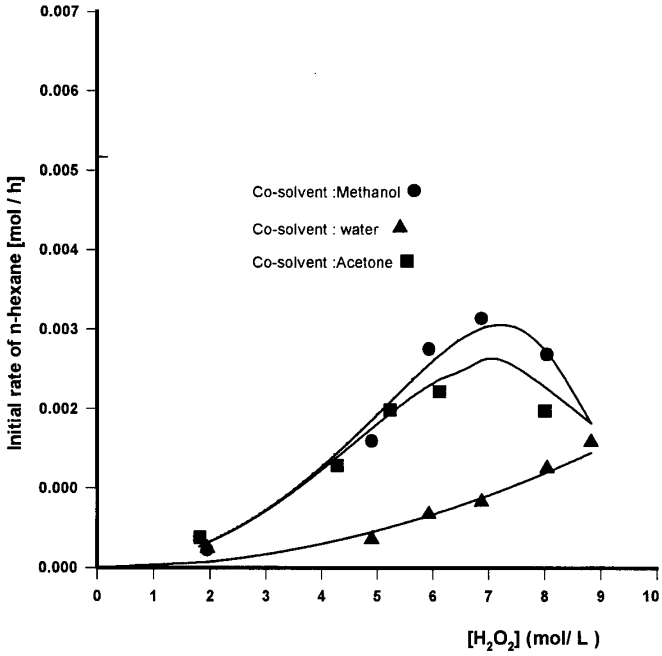

FIG. 3. Initial rate of *n*-hexane consumption versus H_2O_2 concentration. $T = 55°C$. TS-2 catalyst, 500 mg; H_2O_2 (30%), 10 g; *n*-hexane, 20 g. Experimental points: (■) acetone; (●) methanol; (▲) water; lines, predicted values.

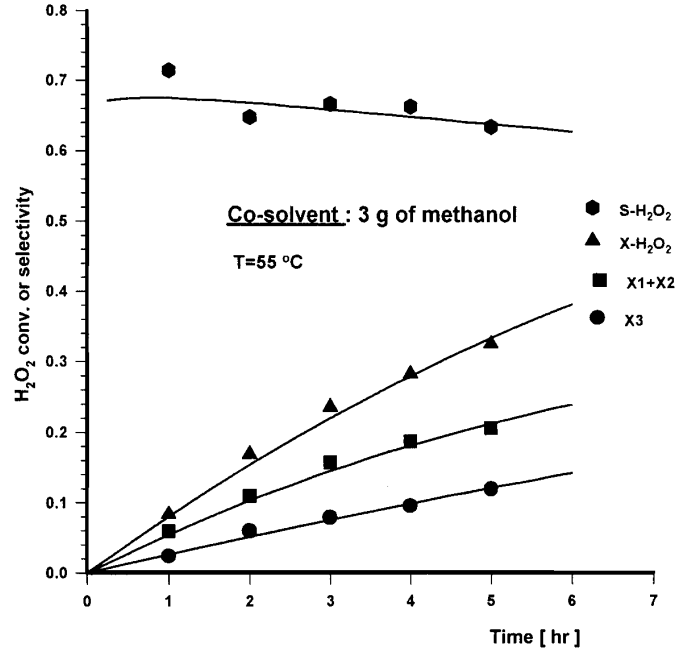

FIG. 4. Partial conversions and selectivity of H_2O_2 versus reaction time. $T = 55°C$. Cosolvent, methanol (3 g). Experimental points: (●) selectivity of H_2O_2; (▲) H_2O_2 total conversion; (■) H_2O_2 conversion to hexanol and hexanone; (●) H_2O_2 conversion according to the decomposition reaction. Lines, predicted values.

with the use of 3 g methanol as solvent at 55°C. It follows from Fig. 4 that the fit of the kinetic model (Eqs. [17]–[19]) with respect to experimental observations is excellent. The validity of the model is also tested as the influence of different kinds and amounts of solvent (methanol, acetone, and water) in the conversion of *n*-hexane during the catalytic oxidation reaction on TS-2 catalyst. The comparison between the computed results and experimental points are illustrated in Figs. 5–7. These results clearly indicate that the kinetic model proposed can describe the catalytic oxidation behavior of *n*-hexane by aqueous H_2O_2 on TS-2 catalyst. It is also observed that the amount of solvents added can modify the reactants concentration. Thus it may be concluded that the effects of the cosolvent on rates and selectivities are entirely explained by the increased solubility of *n*-hexane and dilution of hydrogen peroxide in the aqueous phase and not by any direct action of the solvent on the kinetic constants (19, 24). The kinetic results indicate also that the use of a dual solvent system may have an advantage over a one solvent system, as the result of an increased *n*-hexane solubility without H_2O_2 dilution. Further investigations of this effect are undertaken.

The activation of (2- and 3-)hexanol on TS-2 catalyst surface may follow a Langmuir–Hinshelwood model. The fitted exponent value of (2- and 3-)hexanol concentrations was found to be 0.111. According to the explanations of the terms in Eqs. [17–19], this exponent should be considered representative of the shape of LLE curve. A small exponent corresponds to a large deviation to Henry's law. This low value is in agreement with van der Pol and van Hoof (28) published data. These authors reported that the oxidation of linear alcohols is zero order with respect to the alcohol concentration.

The competitive adsorption of H_2O_2 on the catalyst surface yields some decomposition likely to happen on extraframework titanium sites. The exponent order of $[H_2O_2]$ in Eq. [19] was taken as an adjustable parameter. It is interesting to note that the fitted value of the order of this reaction of H_2O_2 decomposition with respect to H_2O_2 concentration was very close to the theoretical value of 0.5 in Eq. [13]. These results indicate also that the selectivity of H_2O_2 to hydrocarbon oxidation reactions is very much affected at low concentration of aqueous H_2O_2.

The experimental observations of *n*-hexane and H_2O_2 conversions as a function of time for various additions of methanol, acetone, and water are indeed very well predicted by the above kinetic model using the same set of kinetic parameters. This gives credibility to the proposed mechanism and justifies the hypotheses made in deriving the kinetic rate expressions.

CONCLUSION

The present kinetic investigation of selective oxidation of *n*-hexane by aqueous H_2O_2 conducted over a series of

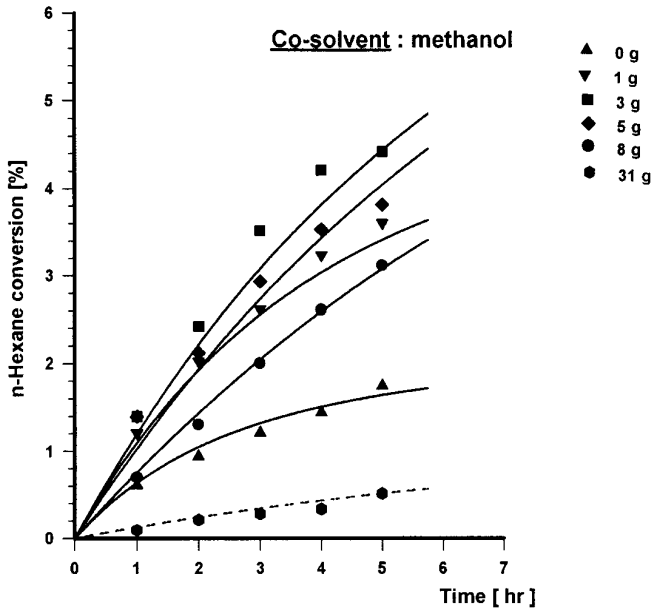

FIG. 5. *n*-Hexane conversion versus reaction time. Temperature, 55°C. Cosolvent, methanol. Experimental points: 0, 1, 3, 5, 8, and 31 g. Lines, predicted values.

different solvents in various amounts on a TS-2 catalyst brings new insights into the catalytic behavior of the oxidation process. The detailed calculations of liquid–liquid phase equilibrium concentrations made allow a much more thorough analysis of the kinetic data and the solvent effects. The maxima observed for the initial rates of *n*-hexane

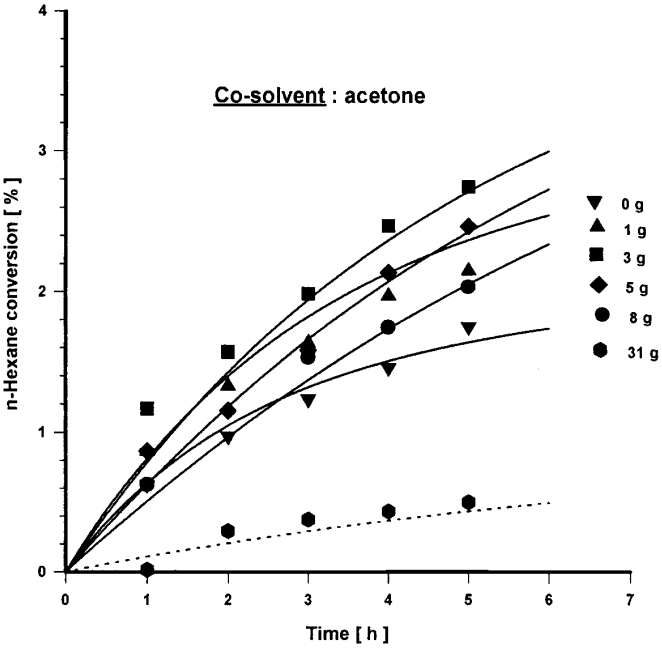

FIG. 6. *n*-Hexane conversion versus reaction time. Temperature, 55°C. Cosolvent, acetone. Experimental points: 0, 1, 3, 5, 8, and 31 g. Lines, predicted values.

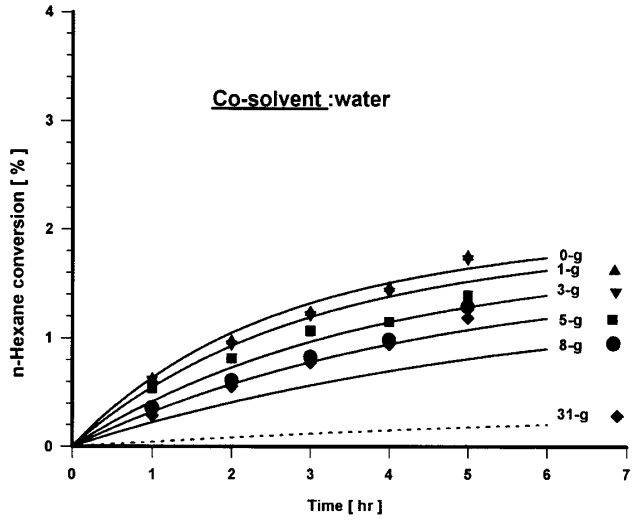

FIG. 7. *n*-Hexane conversion versus reaction time. Temperature, 55°C. Cosolvent, water. Experimental points: 0, 1, 3, 5, 8, and 31 g. Lines, predicted values.

oxyfunctionalization which where previously explained by the limiting effect of *n*-hexane internal diffusion (22) have been given a better explanation. It was indeed shown that the addition of the cosolvent increases the *n*-hexane concentration in the aqueous phase, but decreases the H_2O_2 concentration in this phase, leading to a maximum rate at intermediate cosolvent addition. The new analysis is gaining support from the fact that the same values of the kinetic constants are used in fitting the rate data obtained in absence of a cosolvent as well as in the presence of added methanol and acetone.

APPENDIX: NOMENCLATURE

a	Interfacial area (m^2/m^3)
A_{ij}	UNIQUAC binary interaction parameter (K)
$C_{i,\mathrm{org}}$	Organic phase concentration of component (i)($kmol/m^3$)
$C_{i,\mathrm{a}}$	Aqueous phase concentration of component (i)($kmol/m^3$)
$C_i^{(\mathrm{int})}$	Interface concentration of component (i)($kmol/m^3$)
g^{E}	Molar excess Gibbs free energy (J mol^{-1})
$[i]$	Aqueous phase concentration of component (i)($kmol/m^3$)
k, K	Symbols used for kinetic constants
K	Volumetric aqueous phase mass transfer coefficient
K	Equilibrium partition coefficient
r, R	Reaction rates ($kmol/m^3$ h, kmol/kg h)
R	Universal gas constant (J mol^{-1} K^{-1})
T	Temperature (K)

t	Time of reaction (h)
r, q	Pure species parameters (UNIQUAC)
V_a	Aqueous phase volume (m^3)
V_o	Organic phase volume (m^3)
V_{cat}	Catalyst volume (m^3)
W_{cat}	Catalyst mass (kg)
$[X]$	Active sites or surface intermediates
x_i	Partial conversion of H_2O_2
x_i, z_i	Mole fraction

Greek Letters

α, β, δ	Reference position of C atom
τ	UNIQUAC constant
θ	Area fraction in UNIQUAC model, fractional coverage of active site
ϕ	Segment fraction in UNIQUAC model
ω	Coordination number in UNIQUAC model
γ	Activity coefficient

ACKNOWLEDGMENT

The authors thank NSERC for its financial support of this work through a strategic grant.

REFERENCES

1. Taramasso, M., Perego, G., and Notari, B., U.S. Patent 4,410,501, 1983.
2. Bellussi, G., Carati, A., Clerici, M. G., Esposito, Millini, R., and Buonomo, F., Belgian Patent 1,001,038, 1989.
3. Perego, G., Bellussi, G., Corno, C., Taramasso, M., Buonomo, F., and Esposito, A., *Stud. Surf. Sci. Catal.* **28**, 129 (1986).
4. Boccuti, M. R., Rao, K. M., Zecchina, A., Leofanti, G., and Petrini, G., *Stud. Surf. Sci. Catal.* **48**, 133 (1989).
5. Reddy, J. S., and Kumar, R., *J. Catal.* **130**, 440 (1990).
6. Tuel, A., Diab, J., Gelin, P., Dufaux, M., Dutel, J. F., and Ben Taârit, Y., *J. Mol. Catal.* **63**, 95 (1990).
7. Behrens, P., Felsche, J., Vetter, S., Schulz-Ekloff, G., Jaeger, N. I., and Niemann, W., *J. Chem. Soc. Chem. Commun.* 678 (1991).
8. Reddy, J. S., and Kumar, R., *Appl. Catal.* **58**, L1 (1990).
9. Trong On, D., Bonneviot, L., Bittar, A., Sayari, A., and Kaliaguine, S., *J. Mol. Catal.* **74**, 233 (1992).
10. Millini, R., Previde Massara, E., Perego, G., and Bellussi, G., *J. Catal.* **137**, 497 (1992).
11. Huybrechts, D. R. C., Buskens, P., and Jacobs, P. A., *J. Mol. Catal.* **71**, 129 (1992).
12. Trong On, D., Bittar, A., Sayari, A., Kaliaguine, S., and Bonneviot, L., *Catal. Lett.* **16**, 85 (1992).
13. Tuel, A., and Ben Taârit, Y., *Zeolites* **13**, 357 (1993).
14. Deo, G., Turek, A. M., Wachs, I. E., Huybrechts, D. R. C., and Jacobs, P. A., *Zeolites* **13**, 365 (1993).
15. de Castro-Martins, S., Tuel, A., and Ben Taârit, Y., *Zeolites* **14**, 130 (1994).
16. Tatsumi, T., Nakamura, M., Negeshi, S., and Tominaga, H., *J. Chem. Soc. Chem. Commun.* 476 (1990).
17. Huybrechts, D. R. C., and Jacobs, P. A., *Nature* **345**, 240 (1990).
18. Clerici, M. G., *Appl. Catal.* **68**, 249 (1991).
19. Reddy, J. S., Sivasanker, S., and Ratnasamy, P., *J. Mol. Catal.* **70**, 335 (1991).
20. Huybrechts, D. R. C., and Jacobs, P. A., *Stud. Surf. Sci. Catal.* **72**, 21 (1992).
21. Khouw, C. B., Dartt, C. B., Labinger, J. A., and Davis, M. E., *J. Catal.* **149**, 195 (1994).
22. Fu, H., and Kaliaguine, S., *J. Catal.* **148**, 540 (1994).
23. Bhaumik, A., Kumar, R., and Ratnasamy, P., *Stud. Surf. Sci. Catal. C* **84**, 1883 (1994).
24. Bhaumik, A., and Kumar, R., *J. Chem. Soc. Chem. Commun.* 349 (1995).
25. Pei, S., Zajac, G. W., Kaduk, J. A., Faber, J., Boyanov, B. I., Duck, D., Fazzini, D., Morrison, T. I., and Yang, D. S., *Catal. Lett.* **21**, 333 (1993).
26. Notari, B., *Stud. Surf. Sci. Catal.* **37**, 413 (1987).
27. Huybrechts, D. R. C., Vaesen, I., Li, H. X., and Jacobs, P. A., *Catal. Lett.* **8**, 237 (1991).
28. van der Pol, A. J. H. P., and van Hoof, J. H. C., *Appl. Catal. A. Gen.* **106**, 97 (1993).
29. Abrams, D., and Prausnitz, C., *AiChE J.* **14**, 135 (1975).
30. Lopez, A., Kessler, H., Guth, J. L., Tuilier, M. H., and Popa, J. M., "Proceedings of the 6th International Conference on X-Ray Absorption Fine Structure, York, UK," p. 548. Elsevier, Amsterdam, 1990.
31. Bonneviot, L., Trong On, D., and Lopez, A., *J. Chem. Soc. Chem. Commun.* 687 (1993).
32. Tuel, A., and Ben Taârit, Y., *Appl. Catal. A Gen.* **110**, 137 (1994).
33. Thangaraj, A., Kumar, R., Mirajkar, S. P., and Ratnasamy, P., *J. Catal.* **130**, 1 (1990).
34. Cartier, C., Lortie, C., Trong On, D., Dexpert, H., and Bonneviot, L., *Phys. B* **208** & **209**, 635 (1995).
35. Trong On, D., Kaliaguine, S., and Bonneviot, L., *J. Catal.* **157**, 235 (1995).
36. Le Noc, L., Cartier dit Moulin, C., Solomykina, S., Trong On, D., Lortie, C., Lessard, S., and Bonneviot, L., *Stud. Surf. Sci. Catal.* **97**, 19 (1995).
37. Camblor, M. A., Corma, A., and Pérez-Pariente, J., *J. Chem. Soc. Chem. Commun.* 557 (1993).
38. Khouw, C. B., and Davis, M. E., *J. Catal.* **151**, 77 (1995).
39. Bittar, A., Trong On, D., Bonneviot, L., Kaliaguine, S., and Sayari, A., *in* "Proceedings on the 9th International Zeolites Conference" (R. von Ballmoss, J. B. Higgins, and M. M. J. Treacy, Eds.), p. 453. Butterworth–Heinemann, Boston, 1993.
40. Bellussi, G., Carati, A., Clerici, M. G., Maddinelli, G., and Millini, R., *J. Catal.* **133**, 220 (1992).
41. Clerici, M. G., and Ingallina, P., *J. Catal.* **140**, 71 (1993).
42. Prasad Rao, P. R. H., Ramaswamy, A. V., and Ratnasamy, P., *J. Catal.* **141**, 604 (1993).
43. Geobaldo, F., Bordiga, S., Zecchina, A., Giamello, E., Leofanti, G., and Petrini, G., *Catal. Lett.* **16**, 109 (1992).
44. Tuel, A., Ben Taârit, Y., and Kaliaguine, S., submitted for publication.
45. Aspen Plus Release 8, Flowsheet Simulation, 1989.
46. IMSL Mathematical Software Library, 1989.
47. Yablonskii, G. S., Bykov, V. I., and Gorban, A. N., *in* "Kinetic Models of Catalytic Reactions," Elsevier, Amsterdam, 1991.
48. Majd, A., Ruch, G. E., and Groves, R., *Environ. Sci. Technol.* **24**, 1332 (1990).
49. Nagata, I., *J. Chem. Thermodynam.* **26**, 545 (1994).
50. Zecchina, A., Spoto, S., Bordiga, F., Geobaldo, G., Petrini, G., Leofanti, M., Padovan, M., Mantegazza, M., and Roffia, P., *in* "Proceedings, 10th International Congress on Catalysis, Budapest, 1992" (L. Guczi, F. Solymosi, and P. Tetenyi, Eds.), p. 719. Akadémiai Kiadó, Budapest, 1993.
51. Trong On, D., Le Noc, L., and Bonneviot, L., *J. Chem. Soc. Chem. Commun.,* 299 (1996).
52. Brookhart, M., and Green Malcolm, L. H., *J. Organomet. Chem.* **250**, 395 (1983).
53. Eisenstein, O., and Jean, Y., *J. Am. Chem. Soc.* **107**, 1177 (1985).
54. Munakata, H., Ebisawa, Y., Takashima, Y., Wrinn, M. C., Scheiner, A. C., and Newsam John, M., *Catal. Today* **23**, 403 (1995).
55. Uguina, M. A., Serrano, D. P., Ovejero, G., Van Grieken, R., and Camacho, M., *Appl. Catal. A Gen.* **124**, 391 (1995).
56. Fu, H., M.Sc. thesis, Université Laval, Québec, 1994.